PHYSICAL INITIALIZATION

T.N. Krishnamurti[1]
H.S. Bedi[1]
G.D. Rohaly[1]
D.K. Oosterhof[1]
R.C. Torres[1]
E. Williford[1]
and N. Surgi[2]

[1]Department of Meteorology
Florida State University
Tallahassee, FL 32306-3034

[2]National Hurricane Center
1320 S. Dixie Highway
Coral Gables, FL 33146

Summary: In this overview we present a summary of results on the impact of physical initialization on various aspects of numerical weather prediction. These include the improvements in the nowcasting and short range forecasting skill, the organization of meso-convective precipitating elements as typhoons form; calibration of surface fluxes using the TOGA - COARE data sets during the intensive observation period from its intensive flux array; the improvements in the hydrological budgets during flooding events; the spread reduction for an ensemble of hurricane track forecasts and in an overall improvement of cloud forecasts. The paper concludes with an emphasis on the need for a direct incorporation of the process within four-dimensional variational analysis procedures.

1. INTRODUCTION

The physical initialization procedure developed by Krishnamurti et al. (1991) assimilates 'observed' measures of rain rates into an atmospheric forecast model. During this process the surface fluxes of moisture, the vertical distribution of the humidity variable, the vertical distribution of mass divergence, the vertical distribution of convective heating, the apparent moisture sink (following Yanai et al., 1973) and the surface pressure experience a spin-up consistent with the model physics and the imposed (observed) rain rates.

This is accomplished through a number of reverse physical algorithms within the assimilation mode; these include: a reverse similarity algorithm, a reverse cumulus parameterization algorithm, and an algorithm that restructures the vertical distribution of the humidity variable to provide a match between the model calculated outgoing long wave radiation and its satellite-based observations.

The reverse similarity algorithm is structured from the vertically integrated equations for the apparent moisture sink ($\hat{Q}_2$) and the apparent heat source ($\hat{Q}_1$). A list of acronyms and symbols appear in Table 1. Using the observed rain rates, the surface evaporative fluxes can be obtained from the sum of the apparent moisture sink ($\hat{Q}_2$) and the observed rain rate (P). The surface sensible heat fluxes can also be obtained from a knowledge of the apparent heat source ($\hat{Q}_1$) and the net radiative heating ($\hat{Q}_R$). The

details are presented in Krishnamurti et al. (1991). During the assimilation $\hat{Q}_1, \hat{Q}_2, \hat{Q}_R$ continually evolve from the insertion of the observed rain rates, and the resulting surface fluxes tend to exhibit a consistency with the observed rain rates, which is an important component of the reverse similarity theory (Krishnamurti et al., 1991, 1993, 1994). These fluxes are then used within the similarity theory, and one solves for the potential temperature and the humidity variable (assumed to be unknowns) at the top of the constant flux layer. The assimilation of this data base provides a consistency among the observed rain rates and the surface fluxes; a robust coupling of the ocean and the atmosphere was also seen to result from this approach (Krishnamurti et al. 1993).

The starting point of this analysis is a rain rate input. Figure 1 shows an observed rainfall field based on a mixed algorithm (Gairola and Krishnamurti, 1992). This scheme utilizes a mix of data from polar orbiting satellites, the SSM/I and OLR, and the raingauge observations. The rain rate algorithm utilizes a sharpened OLR based rainfall as a first guess and incorporates the radiometer data of SSM/I into the analysis over the oceanic regions and the surface raingauge data over the land areas. The SSM/I algorithm, we use is based on Olson et al. (1990).

Figure 2 from Gairola and Krishnamurti (1992) describes a flow chart of the components of this algorithm. A first phase of this algorithm addresses a statistical procedure for the sharpening of the OLR rain to the levels of the SSM/I rain. This is done by regression based on a large volume of diverse rainrate data sets over the 10°S and 10°N latitudes. The cirrus anvils of OLR generally produce too much of a broadening of the rainfall signatures when the OLR algorithms are used. The SSM/I based data comes from a number of microwave radiometric channels (85 GHz, 37 GHz, 22 GHz and 19 GHz). This does not exhibit such a cirrus broadening.

The footprint of the SSM/I varies roughly between 35 km^2 to 55 km^2. Thus a much higher resolution rainfall signature is possible from the SSM/I. We have examined three different rain rate algorithms based on the SSM/I data sets; these were developed by Olson et al. (1990), Kummerow and Giglio (1994) and by Spencer (1993). These are essentially based on validation of the use of multi-channel SSM/I data against ground truth provided by surface based measurements from radar and rain gauges. The global tropical precipitation intensity amounts were quite different in these approaches. These are illustrated in Figures 3a, b, c, where we show an example of the rainfall distribution from three algorithms. It is interesting to note the current uncertainties in the rainfall measurements, the mutual tropical correlations of these fields are of the order of 0.6. We noted that when we carried out the physical initialization using these three fields to define the initial distributions, we experienced a somewhat different response from the three methods in medium range forecasts. It is apparent that further work is needed to improve the satellite based rainrate algorithms.

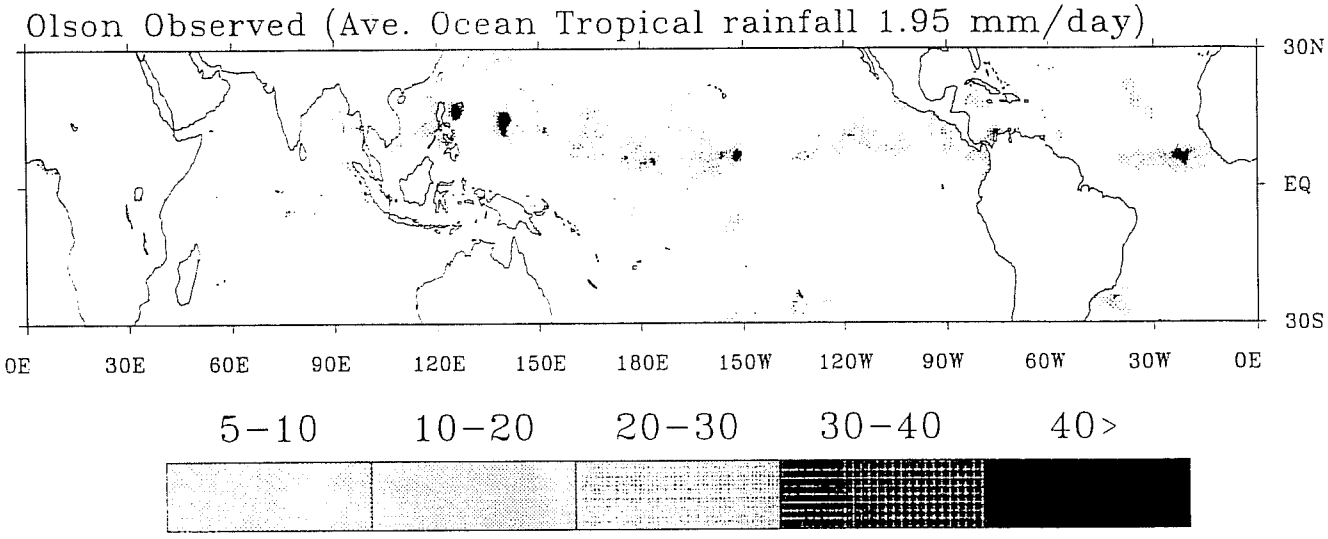

Fig (1) An example of rainfall for a 24 hour period (mm/day) based on the mixed (SSM/I, OLR, raingauge) algorithm.

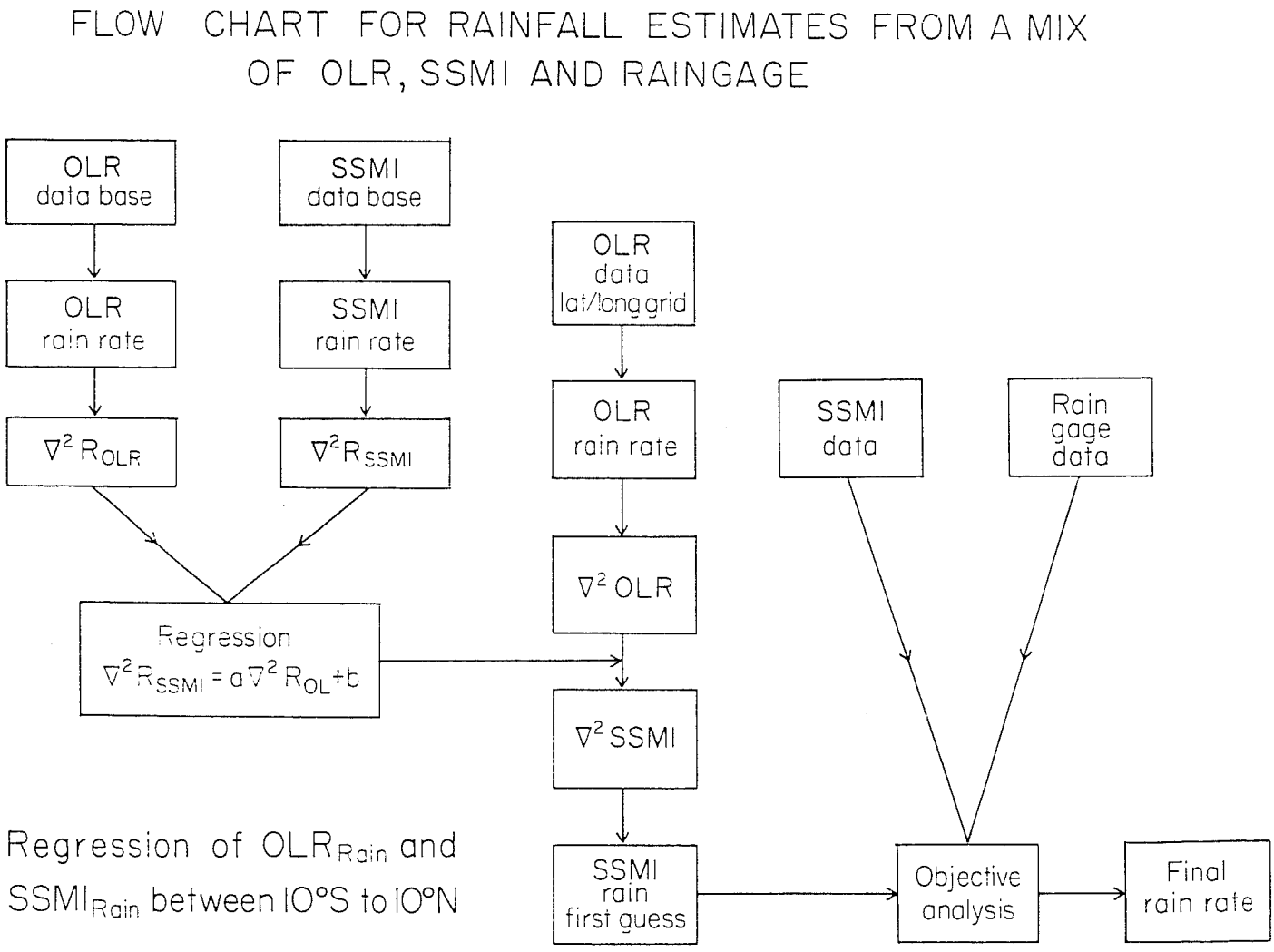

Fig (2) Flow chart for the mixed rain rate algorithm OLR, SSM/I raingauge.

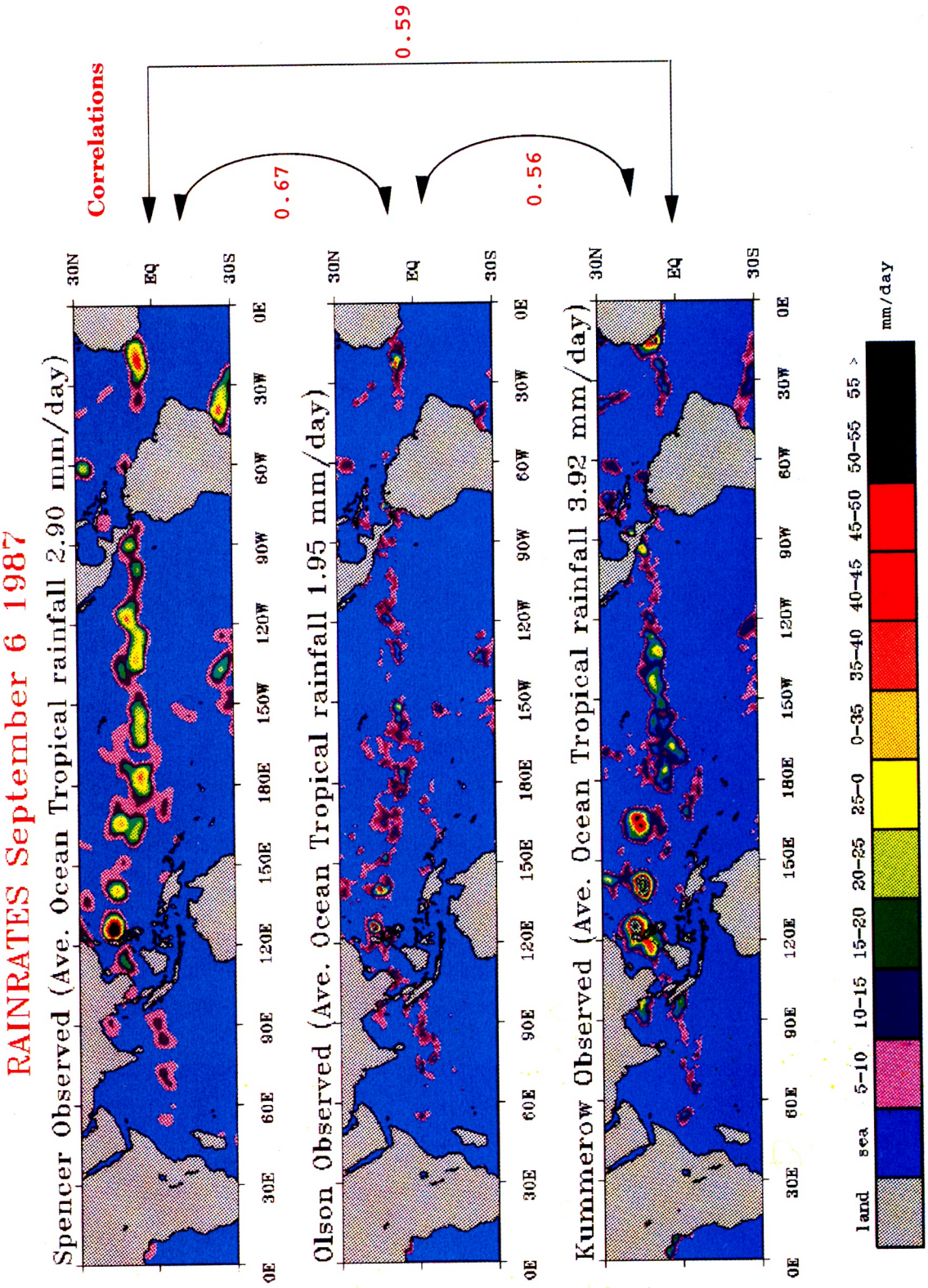

Fig (3) 24 hour rainfall total based on three rain algorithms, units mm/day.
a) Spencer (1993), b) Olson et al. (1990), c) Kummerow and Giglio (1994)

The model rainfall is a function of horizontal resolution; in that context we found some rainrate algorithms were better suited than others for high resolution global model integrations. There are important hydrological constraints on the globally averaged measures of surface evaporation and rainfall. Global average rainfall values such as 2.75 mm/day are generally accepted from global hydrological considerations. In that context we found some algorithms were better suited than others for describing the global budgets. Based on these considerations, we have been largely using the algorithms of Olson et al. (1990) algorithm over the oceanic portions. The land area rainfall description has been based largely on raingauge observations and the sharpened OLR rainfall estimates. The sharpened OLR provides a first guess of the global tropical rainfall for our analysis.

A regression of the laplacian of the OLR algorithm rain rates and the laplacian of the SSM/I based (and collocated) data sets between 10°S and 10°N were used to define a sharpening function. Thus, given the OLR and the SSM/I based rainfall distributions, a regression among these two provides a sharpening of the laplacian of the OLR rain and the inverse problem, i.e. the solutions of the poisson equation, in turn, provides the sharpened rain. That process is defined in the left hand side of the flow chart, Figure (2) . Thus given the data sets of the OLR, SSM/I and the raingauge for a particular period were carried out, following Gairola and Krishnamurti (1992). This sharpened OLR rainfall covers the entire tropical belt between 30S and 30N. The SSM/I based rainfall on satellite swaths over the oceanic regions plus the raingauge estimates from the surface reports over land areas were next objectively analyzed to obtain the final rain rate descriptions. Space-time bins, 6 hours in time and a spectral transform grid square in space, define the resolution of the 'observed' rainfall which is assimilated via the physical initialization procedure.

2. RAINFALL PREDICTION SKILL

If we follow a sequence of OLR matching, reverse similarity and a reverse cumulus parameterization within an assimilation, we find a major improvement in the nowcasting and one day forecasting skill of rainfall (Krishnamurti et al. 1994). We had performed the physical initialization for the entire month of October 1991 at a resolution T106 for our global model which is outlined in the appendix of this paper.

The month long skill of rainfall initialization is shown in Figure (4a), Krishnamurti et al. (1994). A much higher skill (of the order of 90%) compared to those of real time operations can be seen here. In fig. 4b we show the one day forecast skill. We find that the use of physical initialization leads to much higher one day forecast correlations, i.e. of the order of 60% for this ensemble of 30 forecasts. This compares with a skill of roughly 35% for the one day forecasts from the various operational centers and those for the persistence and for a control experiment conducted with the FSU model, where no physical initialization was invoked.

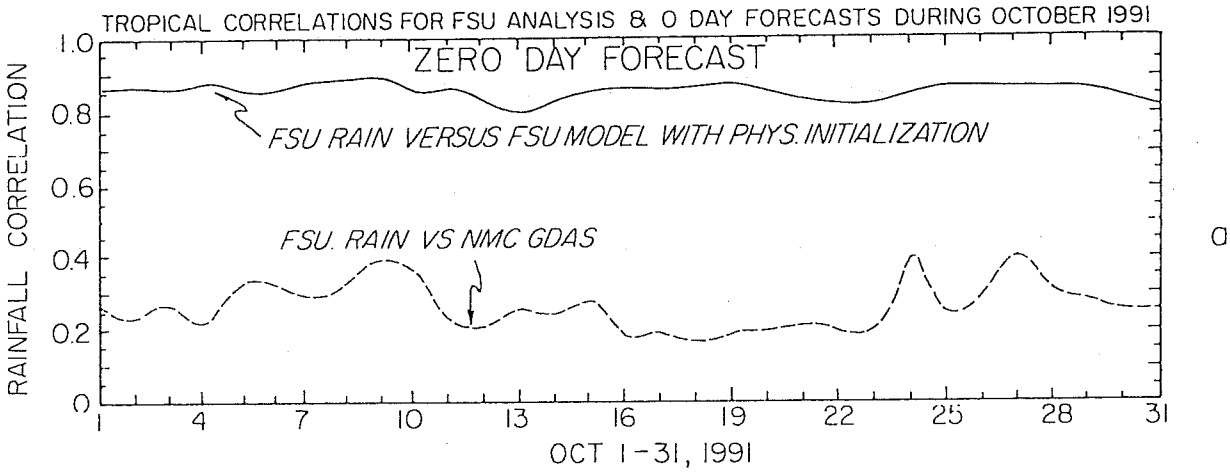

a

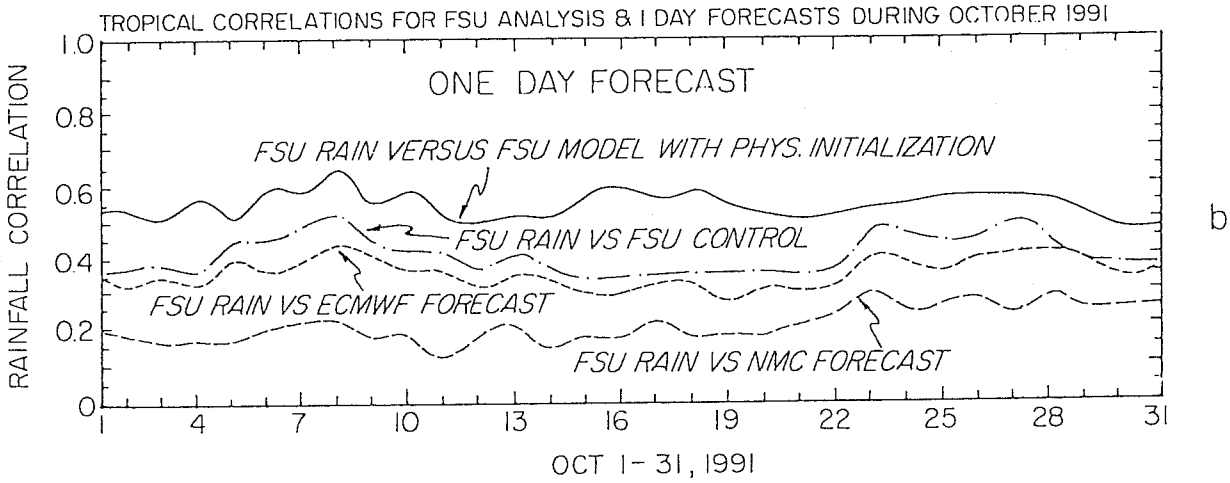

b

Fig (4a) Month long skill i.e. correlation of predicted and observer rain over the tropical belt for the FSU model (based on physical initialization) for day 0, also shown is the skill of the NMC/GDAS rain compared to observed rain.

Fig(4b) Month long skill i.e. correlation of predicted and observed rain over the tropical belt, 30°S to 30°N, for the FSU (physically initialized and control), NMC and ECMWF models for the one day forecast.

There appears to be only a marginal improvement in useful skill for rainfall forecasts from the physical initialization on forecasts beyond two days.

3. TOGA-COARE FLUXES

Calibration of model based surface fluxes to some rich data base such as those provided by TOGA-COARE is desirable for the physical initialization.

During the field phase of the TOGA-COARE the intensive observation period (IOP) included November 1992 through February 1993. Within this period an intensive flux array (IFA) that provided oceanic surface fluxes over the warm pool of the tropical Pacific ocean was set up for higher resolution observations. This special data set was useful for the calibration of model-based estimates of surface fluxes. The intensive flux array is located within the warm pool close to the equator (2°S, 156°E). A polygonal array of observational sites, weather stations at Kapingawa range and Kavieng and ships located at (2°S, 158°E), (4°S, 155°E) and at the center (2°S, 156°E) constitute the IFA. An integrated sounding systems (ISS) is part of the flux array; it includes a profiler, a radio acoustic sounding system, an omega based Navaid sounding system and an enhanced surface station, Parsons et al (1994). A total of six ISS were implemented during the TOGA-COARE IOP phase.

Physical initialization includes a reverse similarity theory within its precipitation assimilation. Over most of the transform grid points of the global model the vertical integral of the apparent moisture sinks following Yanai (1973), provides a measure of the surface flux of moisture over the rain areas, i.e.

$$\hat{Q}_2 = \hat{E} - \hat{P}$$

Given an estimate of precipitation from the satellites and raingauge, the assimilation constantly improves the estimates of $\hat{Q}_2$ and E.

In order to provide a consistency among precipitation and evaporation we use a reverse similarity theory, Krishnamurti et al. (1991) to calculate the data on top of the constant flux layer that makes use of the aforementioned Yanai fluxes. Assimilation of this data brings about this consistency. However, several modeling approximations implicit in the surface similarity theory show parameter sensitivity to the modeled fluxes. The depth of the constant flux layer is one such parameter. It is possible to calibrate an optimal value of this depth with respect to the data from the intensive flux array. Fig (5) illustrates a comparison of TOGA-COARE fluxes with those for our model.

4. THE IMPACT OF PHYSICAL INITIALIZATION ON IMPLICIT CLOUD FORECASTS

In many numerical weather prediction models the cloud-radiative interactions are carried out from an implicit definition of cloud fractions. Clouds are defined to exist if the relative humidity at a model level

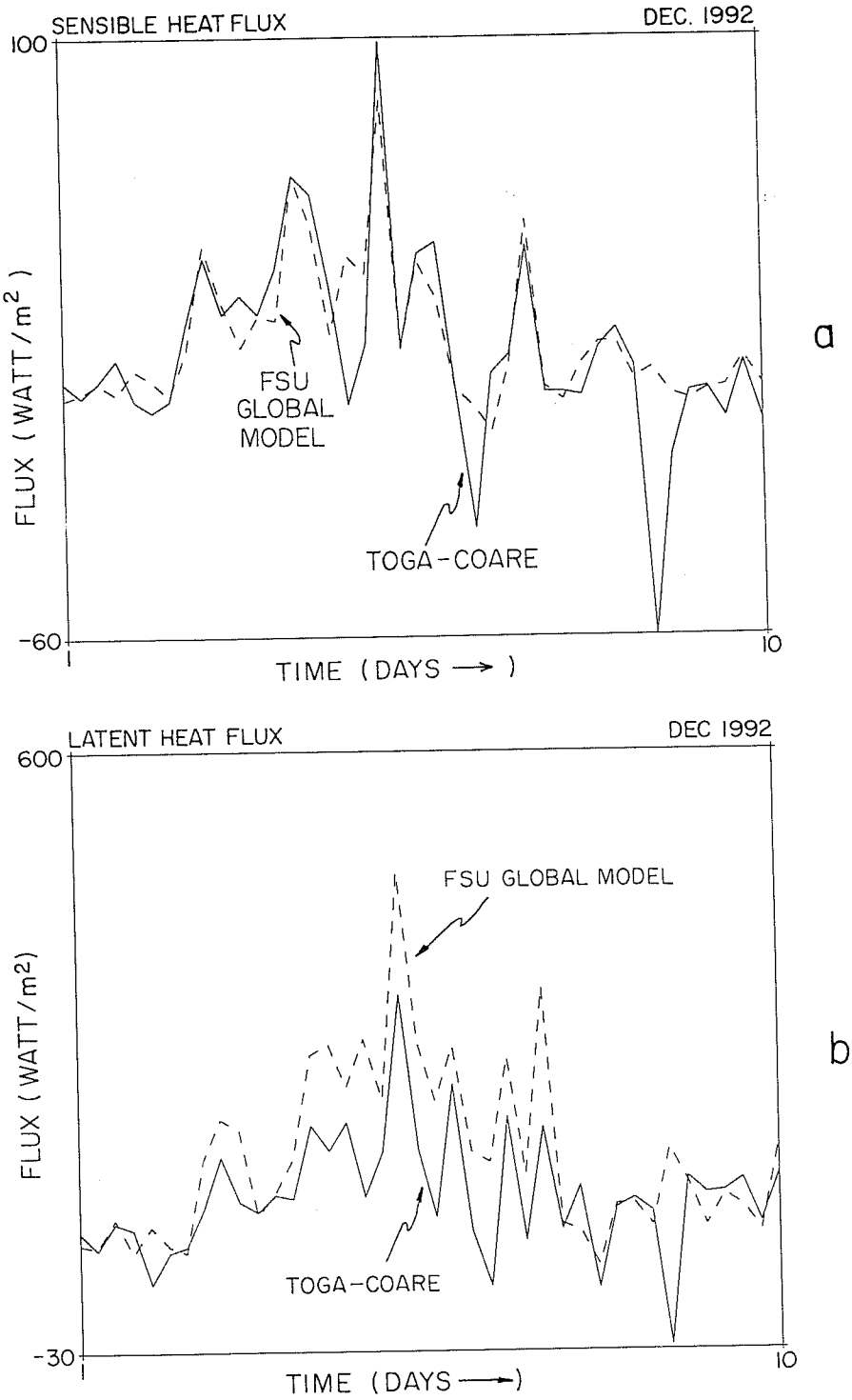

Fig (5) TOGA fluxes

exceeds a threshold value (usually called a critical relative humidity). These threshold values are usually determined by examining the satellite measures of outgoing longwave radiation for clear line of sight, low, middle or high cloud targets. Therefore, with collocated temperature/ humidity soundings, one can find the prevailing humidities during occurrences of low, middle or high clouds. The Nimbus 7 satellite data and the FGGE soundings have been used to define these threshold values globally, Lee and Krishnamurti (1994).

The humidity analysis is one of the weakest components of data assimilation at operational analysis centers. The first guess field is based on the model forecast and the available radiosonde stations provide the real time data, which in fact are very sparsely distributed over the tropics. This leads to large uncertainties in the coverage of low, middle and high clouds. The model-based definition of the net outgoing longwave radiation, as a consequence, is subject to large errors from the misrepresentation of clouds. Within the physical initialization, a matching of the model calculated and the satellite observed OLR is accomplished. The vertical structure of the humidity variable in the upper troposphere, where the humidity observations are sparse and unreliable, are defined by a single parameter structure function. This parameter is determined from a minimization of the difference between the satellite and the model OLR values using a bisection method. Lacking a more sophisticated approach this simple method has been found to be fairly useful in improving the humidity analysis over the upper troposphere.

Figure (6 a, b, c) shows an example illustrating the improvement in the definition of the outgoing longwave radiation field. Panel a) shows satellite observations; Panel b) shows a control run which did not include the physical initialization; Panel c) shows the results from the physical initialization experiment. These results, Krishnamurti et al. (1991), demonstrate that this method produces a close match of the observed and the model OLR, see Figures (6 a and c). The correlation coefficients of the OLR (satellite) and the OLR (control) is 47%; whereas the correlation coefficient of the OLR (satellite) and the OLR (physical initialization) is 97%.

Physical initialization, as a consequence, appears to provide a strong positive impact on the prediction of clouds. This is apparent from the root mean square errors of the predicted low, middle and high clouds. The question arises as to how we should define an observed cloud fraction? Since physical initialization produces a much superior initial OLR field, it seems reasonable that the observed cloud fraction should be calculated from physically initialized fields for the respective forecast verification periods. Figure (7) shows the spin-up of clouds for the control and physical initialization experiments. A near constancy of the forecast skill of the middle and high clouds throughout the forecast period was noted for the physically initialized experiment. The low cloud fractions continue to exhibit a spin up even after the physical initialization was invoked. That is understandable because these low clouds are largely nonprecipitating and are not handled by our procedure. Further work is needed to improve the initialization

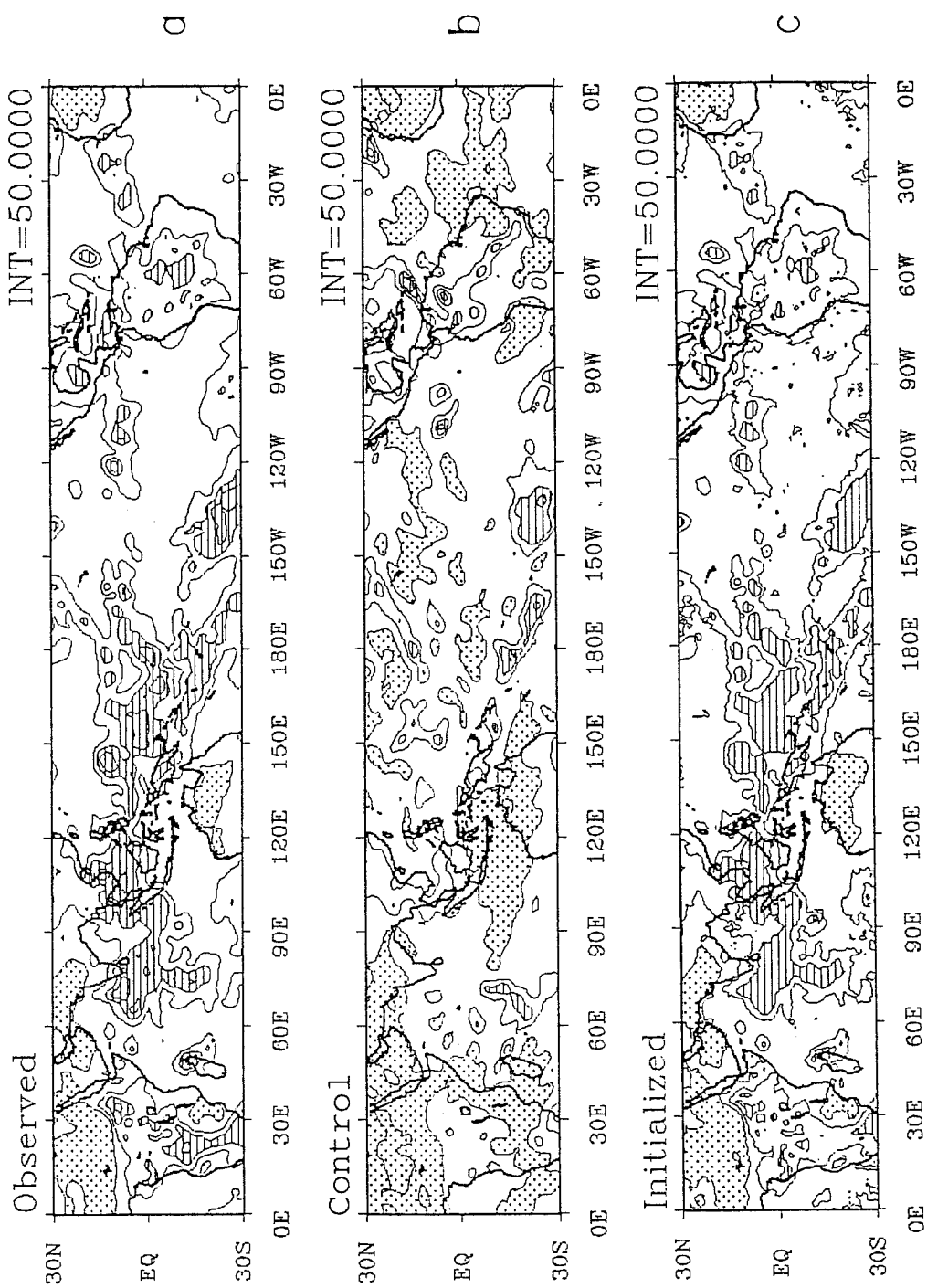

Fig (6) Typical Initial OLR fields from
a) satellite;
b) control run that does not include a physical initialization
c) physical initialization; Units: watts/m^2.

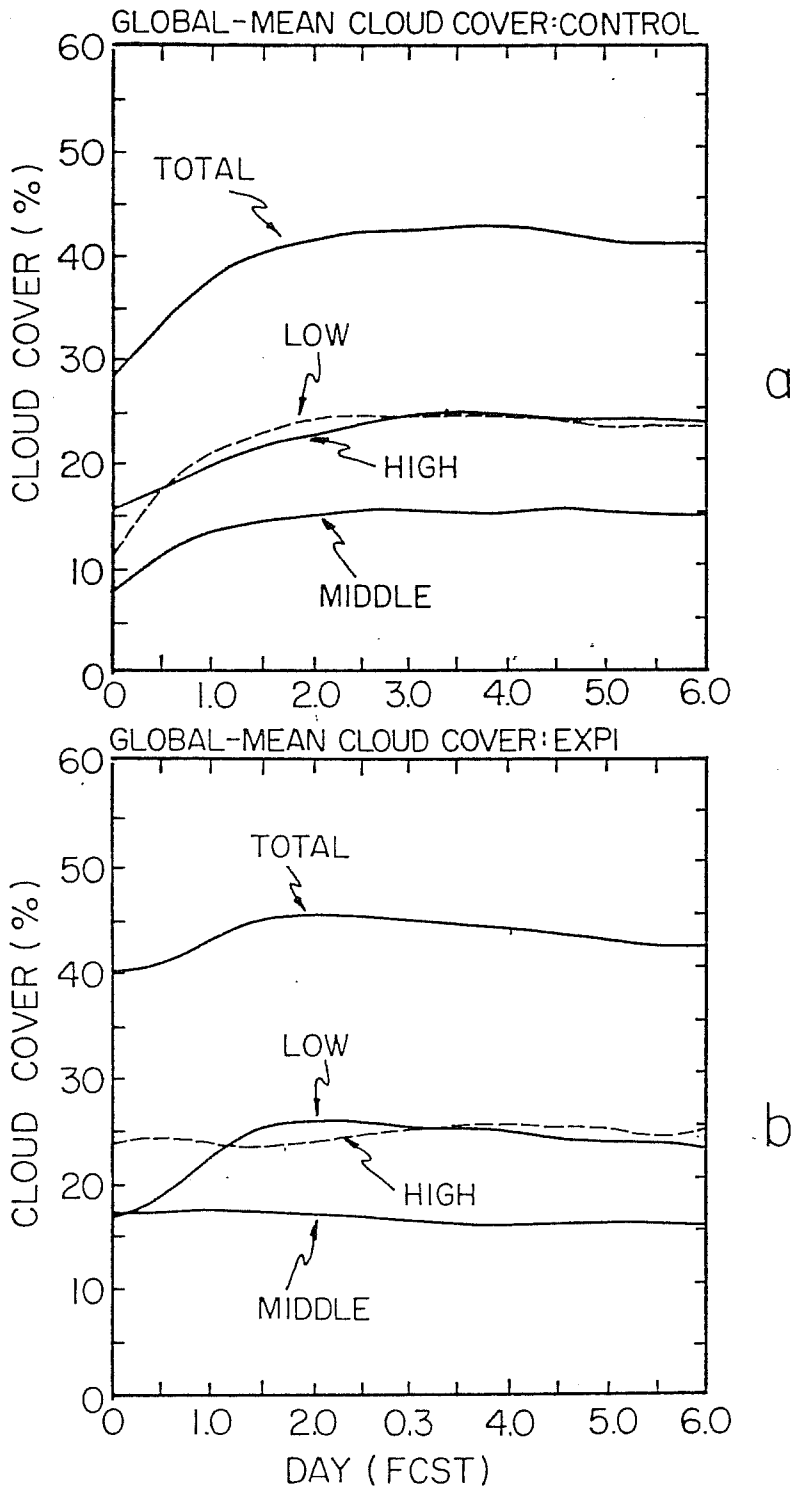

Fig (7) Spin up of the fractional cloud cover for the a) control and b) the physical initialization experiments. Low, middle and high cloud fractions are illustrated.

of low cloud fractions. The treatment of shallow convection parameterization which is based on a simple formulation of diffusion for heat and moisture, Tiedke (1984). The control experiment, however, did exhibit a spin-up for these cloud fractions. The predicted skill of total cloud cover for the control and the physical initialization (normalized with respect to persistence error) are shown in Figure 8. A value greater than one denotes a skill less than persistence. The control experiment appears to have a useful skill of roughly 1.5 days whereas the physical initialization appears to improve this situation to roughly 3.5 days. Prediction of cloud cover is apparently one of the most difficult areas of medium-range prediction. The move toward the explicit handling of clouds, rather than their definition via threshold relative humidity appears to be the new approach nowadays. That relies on the definition of the formative and dissipative processes for convective and non-convective clouds. These are areas where further work will be required prior to their assessment within physical initialization.

5. SIGNATURES OF MESO-CONVECTIVE SYSTEMS

For a long time observations from satellite, aircraft and radar have revealed the amplification of tropical disturbances from the organization of tropical convection. This organization of convection, in fact, appears to occur on meso-convective scales. If the placement of meso-convective systems organizes into a quasi-circular geometry, then an intensification of the zonally symmetric scale (wave number zero) about a local cylindrical frame of reference is possible. In the tropical latitudes (roughly between 5 and 15 degrees off the equator), given a low level cyclonic vorticity, warm SST's ($\geq 27°C$), weak vertical shear of the horizontal wind, such an organization of deep convection generally contributes to the generation of available potential energy and its conversion to kinetic energy with an amplification of axially symmetric motions. When we perform physical initialization at a very high resolution, such as T213, it is possible to retain the meso-scale signatures of rainfall as seen from the SSM/I. The transform grid separation at this resolution (T213) is comparable to the footprint of the radiometers of the SSM/I instrument.

Figure (9 a,b,c) illustrates a typical match between the 'observed', the 'physically initialized' and the 'control experiment' based rainfall results at the resolution of T213. The model is able to initialize almost all of the meso-convective precipitating elements. There were roughly 47 elements around the global tropics on this date (June 22, 1992). The tropical correlation of the initialized rain, with respect to the observed rain, over all of the transform grid squares is of the order of 0.9. On the other hand the correlations for control experiments that do not invoke physical initialization is around 0.35.

Each of these mesoconvective elements are initialized by the physical initialization algorithm. Each of these systems appear to acquire a robust vertical structure from the physical initialization. Shown, in figures 10, 11, 12 and 13, following Krishnamurti et al. (1995), are some examples of mesoscale structures of the various precipitating elements of Figure (9). Figure (10) illustrates results for an element

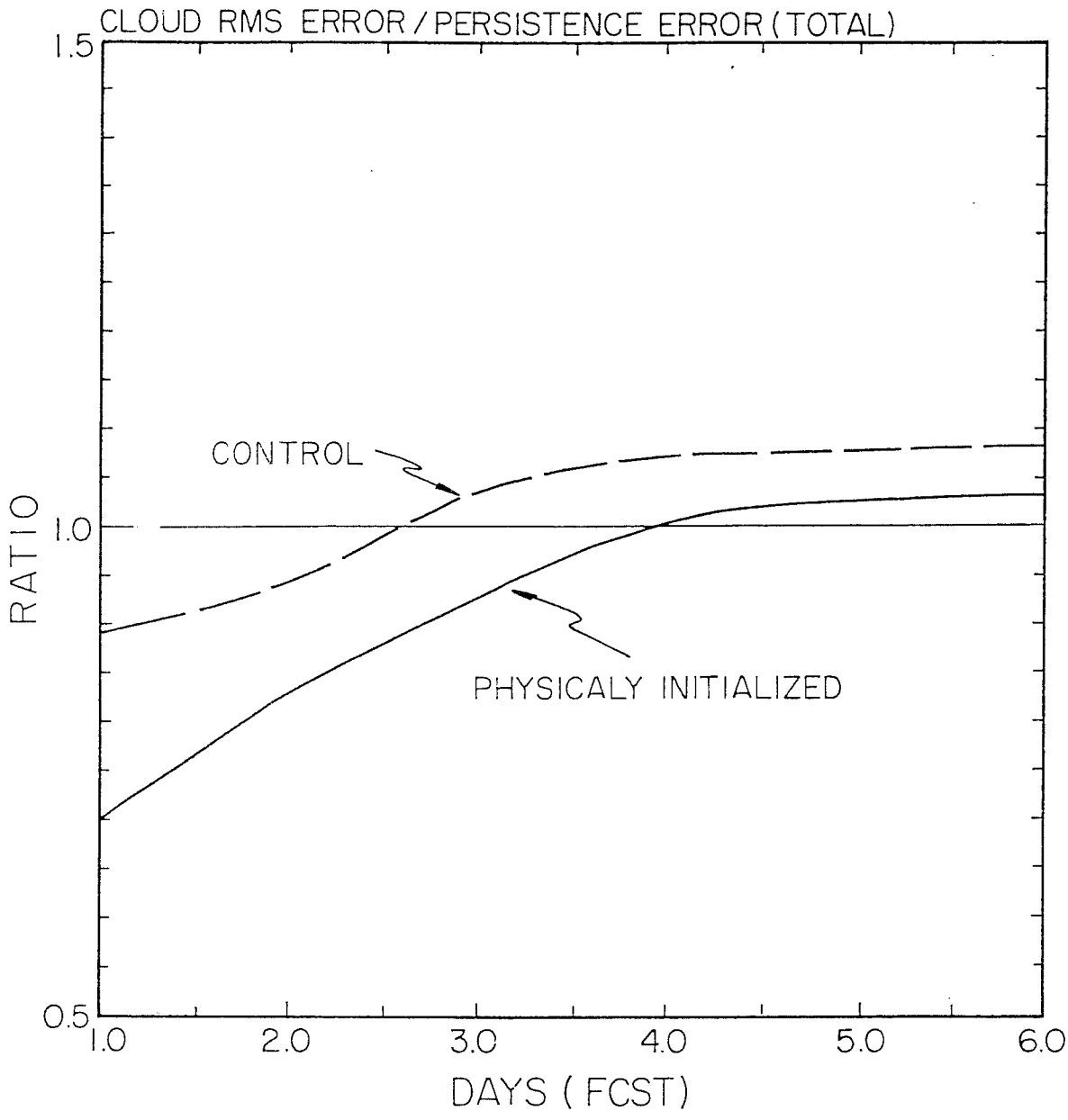

Fig (8) Predicted skill, normalized to that of persistence, for the total cloud cover is shown against the forecast days. A value greater than one denotes a skill less than that of persistence. Results for the control and the physical initialization are shown here.

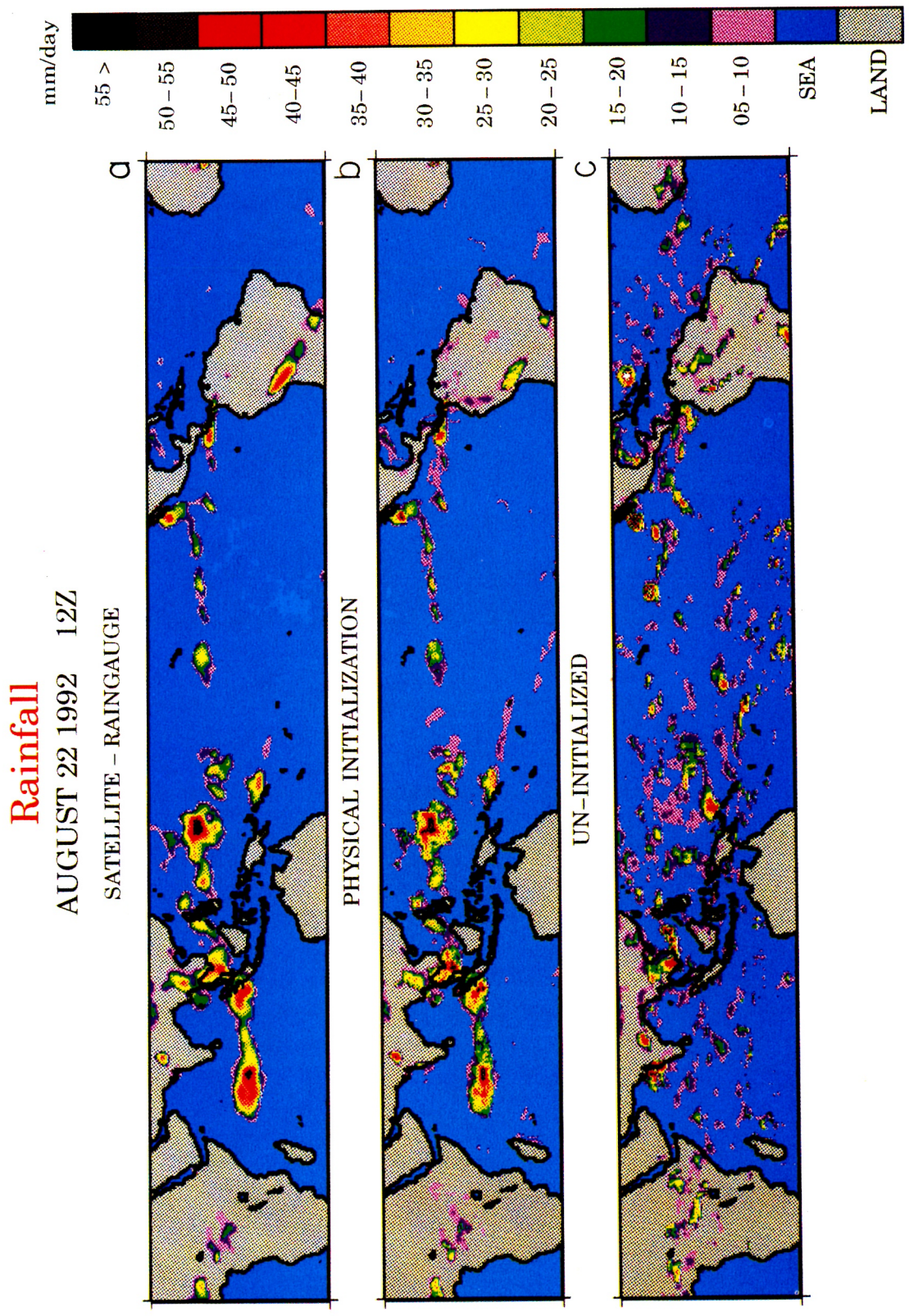

Fig (9) a) Observed (based on SSM/I, OLR and rain gauge) rainfall for a 24 hour period.
b) Physically initialised rain for the same 24 hour period.
c) Control experiment based rain for the same period. Units: mm/day.

over the northern end of New Guinea. This element is located close to the equator around 140°E. The control run describes a straight flow, Figure (10a) at the 850 mb surface. This region is located to the west of the south Pacific convergence zone. In panel b, the flow field at 850 mb based on physical initialization illustrates a near equatorial vortical circulation. Also superimposed on this panel are the initialized rain rates (maximum rainfall is of the order of 43 mm/day). The winds respond to the heating and a vertical circulation results. A marked change in the initial circulation results from the physical initialization. Figure (10) also illustrates the vertical profiles of vertical motion and relative vorticity over the mesoscale precipitating area for the control and for the physically initialized experiments. It is apparent that these precipitating clusters in the physical initialization experiment imply a more robust lower tropospheric convergence, a strong upper tropospheric divergence, stronger upward motions, slightly enhanced positive relative vorticity over the lower troposphere and a somewhat enhanced negative relative vorticity in the upper troposphere. Figure (11) illustrates another similar sequence for a mesoscale precipitating cluster over India for August 22, 1992, 1200 UTC. Panels a, b and c show a robust initial response for the mesoscale divergence, vorticity and vertical motion from the physical initialization (solid lines); the dashed lines show the initial results from the control experiment where the mesoscale precipitation was absent. The flow field at 850 mb (panel d) for the control run shows a basic northerly flow. The initial rainfall amounts implied by the control run are of the order of 0.5 mm/ day. When the precipitation input is introduced via physical initialization, the initial flow field exhibits a cyclonic circulation (shown in panel e). The superimposed rainfall rates are of the order of 53 mm/ day, which developed a strong divergent wind response defining what looks like a mesoscale monsoon depression. The panel e shows an analysis, based on delayed data from the India Meteorological Department which was valid for 22 August, 1992 at 1200 UTC. Overall we note that the physical initialization can improve data deficiencies of the operational data sets. In a recent paper on these mesoscale signatures of physical initialization (Krishnamurti et al., 1995), we have illustrated several such examples around the global tropical belt. Basically the entire tropical analysis is modified by the physical initialization from the introduction of meso-convective precipitating elements.

The occasional organization of meso-convective elements is another important aspect of very high resolution global modeling. As we proceed westward along the undisturbed trades we see a gradual build-up of towering cumulus and the occurrence of meso-convective elements. The low-level circulation tends to advect (sweep) and organize these elements. Developing tropical systems tend to advect and thus organize these elements into synoptic scale systems. Inner convection tends to draw the outer air from great distances and mesoscale intensification occurs from the angular momentum principle i.e. spin up of the rotational flow at the inner radii. Although angular momentum is not conserved due to losses from pressure and frictional torques, hurricane development does seem to follow along these lines. We can in fact

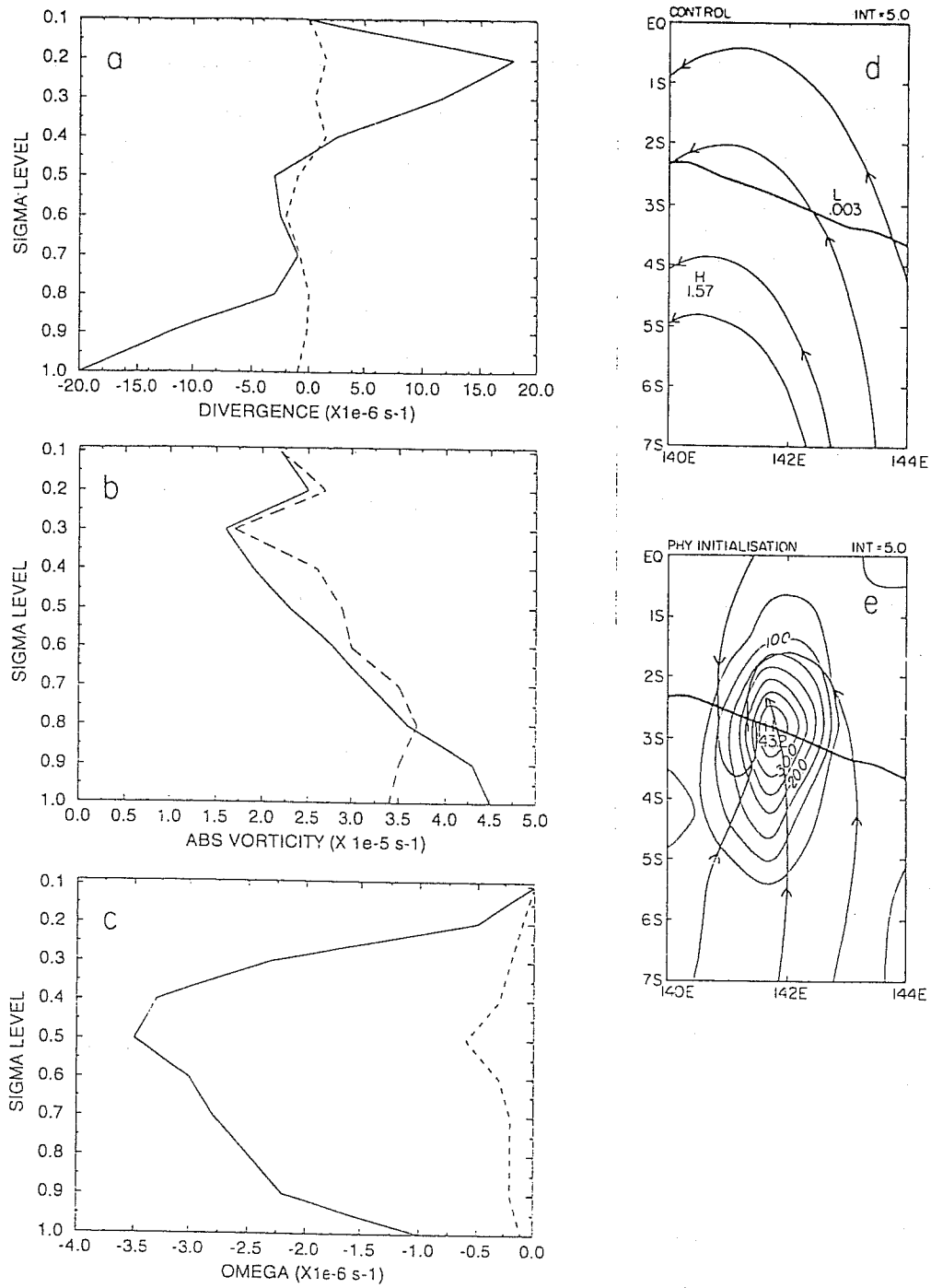

Fig (10) Structure of a meso-convective element near New Guinea, 22 August 12 UTC, 1992.

a) Vertical structure of divergence with (solid line) and without (dashed line) physical initialization.

b) Vertical structure of absolute vorticity with (solid line) and without (dashed line) physical initialization.

c) Vertical structure of vertical velocity omega with (solid line) and without (dashed line) physical initialization.

d) Initial 900 mb streamlines for the control experiment without physical initialization. Weak initial rainfall amounts mm/3 hrs are highlighted for the control experiment.

e) Initial streamlines (with arrows) for the experiment with physical initialization. Also shown is the physically initialized rainfall (mm/3 hrs).

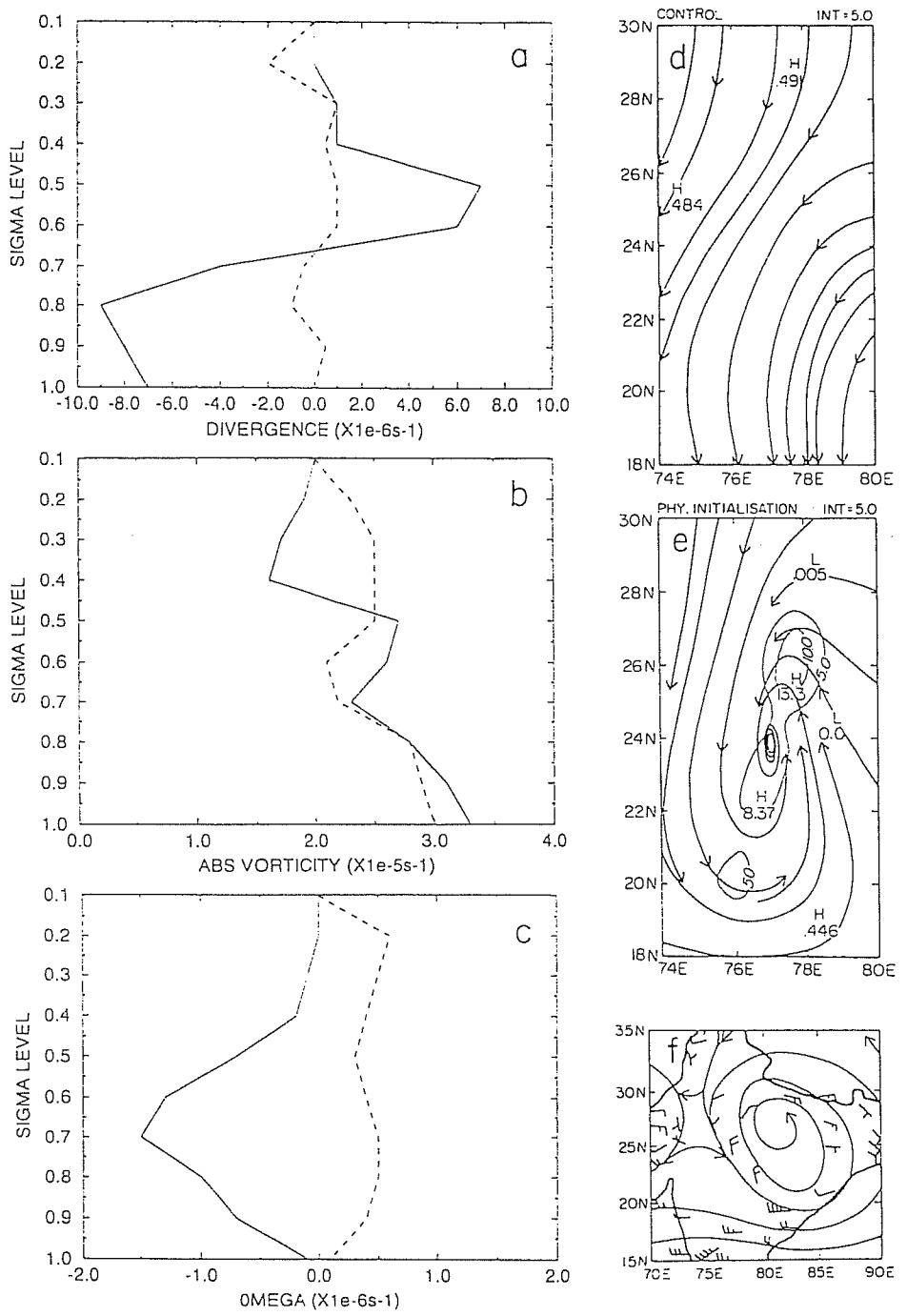

Fig (11) The structure of a meso-convective element over north-central India at around 24N and 77E on 22 August 12 UTC, 1992.

a) Vertical profile of divergence with (solid line) and without (dashed line) physical initialization.

b) Vertical profile of absolute vorticity with (solid line) and without (dashed line) physical initialization.

c) Vertical profile of vertical velocity with (solid line) and without (dashed line) physical initialization.

d) Flow field at 900 mb derived from operational analysis at ECMWF. The initial rainfall amounts 0.484 and 0.491 mm/3 hrs show the maximum rainfall over northern India for the control experiment.

e) Flow field at 900 mb obtained after physical initialization. A monsoon depression is clearly evident in this analysis. The initialization rain (mm/3 hrs) is superimposed.

f) 850 mb weather map obtained from India Meteorological Department for 22 August 1992 at 00 UTC. The depression is located near 80E and 27N. The observed winds are plotted at station locations.

illustrate much of this line of thinking from the detailed output of very high resolution global models. We shall next illustrate some results of global prediction experiments carried out at the resolution T213.

Figures (12 a through e) illustrate the motion (sweeping), coalescence, decay and new formations of meso-convective precipitating elements. This sequence illustrates rainfall forecasts (with superimposed 850 mb predicted streamlines) at intervals of 6 hours between hours 30 and 48 of forecast. Typhoon Omar formed over the tropical Pacific ocean from a tropical depression during this period of the forecast. The predicted amplitude of the 850 mb wind increased from 15 ms-1 to 23 ms-1 during this period. The precipitating mesoscale elements clearly exhibit an organization as the storm develops. We shall next study the longer time history of a single element. A cluster, denoted as number 1, was followed during a period as it moved from the trade wind circulation into the storm circulation. The vertical distribution of divergence, vertical motion and vorticity between hours 30 and 48 for the meso-convective precipitating element 1 are shown in Figure (13). We note that the vertical motion increases considerably as the cluster moves into the storm's circulation. The lower tropospheric convergence and the upper tropospheric divergence amplify during this transition. The meso-scale vorticity does not seem to exhibit an analogous increase Krishnamurti et al. (1995). This was an important result. In a series of recent articles, based on the shallow water equations, it was demonstrated that meso-scale vorticity could be swept by the circulations of a larger scale vortex, leading to the intensification of the latter, Holland and Dietachmayer (1993), Lander and Holland (1993), Richie and Holland (1993). Our global model studies did not exhibit such a behavior for the vorticity of individual mesoscale elements Krishnamurti et al. (1995). The storm (Omar) did intensify from the sweeping of the divergence, vertical motion and heating of these mesoscale precipitating elements. The organization of these elements into a circular geometry enhances the lower tropospheric convergence for the axially symmetric mode (wave number 0 for a local cylindrical frame of reference), the covariance of convergence and vorticity on this scale leads to the intensification of the storm vorticity. In the present global model at the resolution T213 we note more of a direct thermodynamical role for these meso-convective precipitating elements. This of course needs to be looked at further with high resolution meso-convective nonhydrostatic models with detailed microphysics. We also noted, after examining many of these meso-convective precipitating clusters, that the magnitude of divergence was in general larger than the magnitude of the relative vorticity on these scales.

We also noted that a resolution such as T213 was necessary to resolve the meso-convective precipitating elements, we did not see such individual meso-convective precipitating clusters at the resolution T106, and they were poorly defined at the resolution T170. Figure (14 a,b and c) illustrates the physically initialized rainfall at the resolution T106, T170 and T213. We note a gradual improvement in the definition of meso-convective elements as we initialize at the higher resolutions. Initially the rainfall over the oceans on this scale as defined from the SSM/ I radiometric data was closely initialized because of

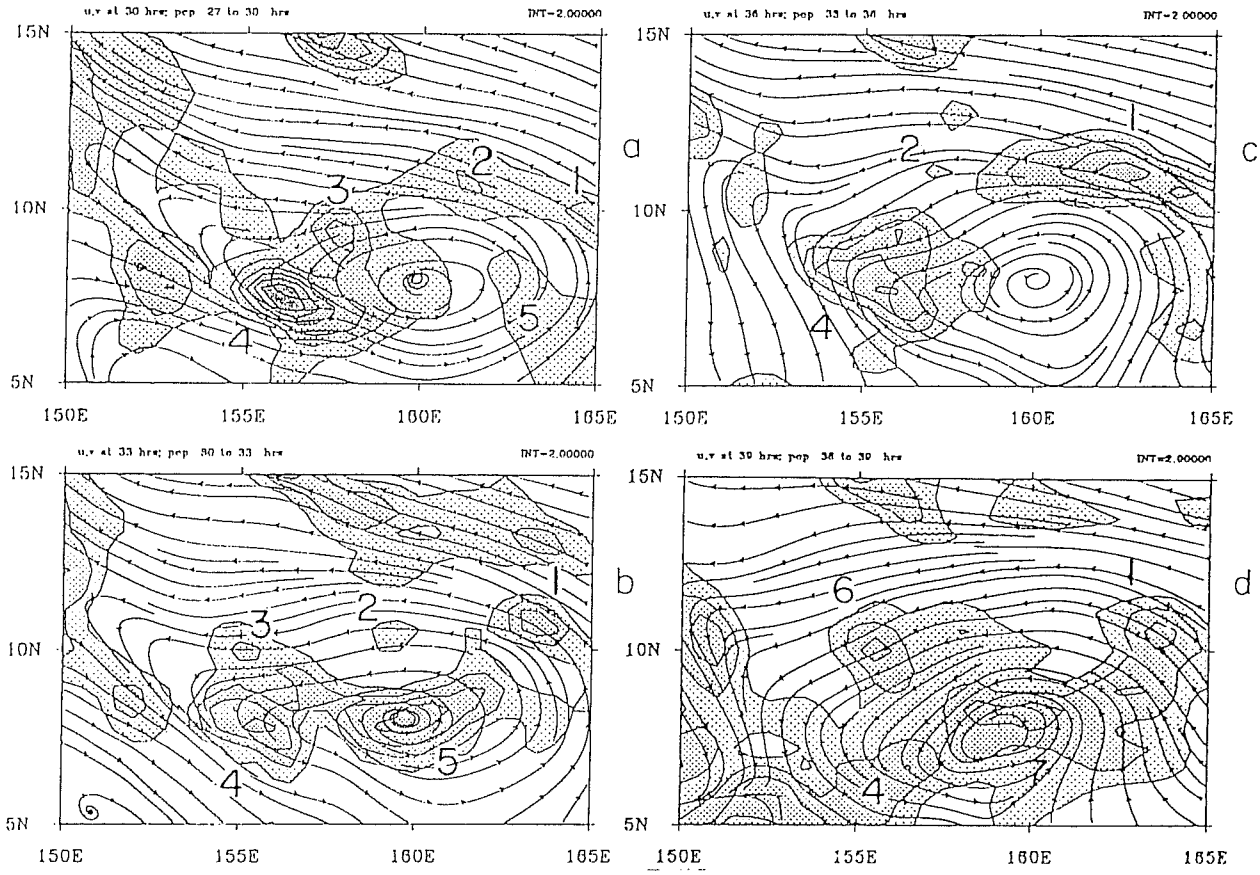

Fig (12) (a through g) Flow field at 900 mb at intervals of 3 hours between hours 30 and 48 hours of forecast. Superimposed are the precipitation (mm/3 hrs), interval of analysis 2 mm/3 hrs. The meso-convective elements are identified by numerical labels. Shading scales for rainfall identified below figure.

TYPHOON OMAR
AUGUST 1992

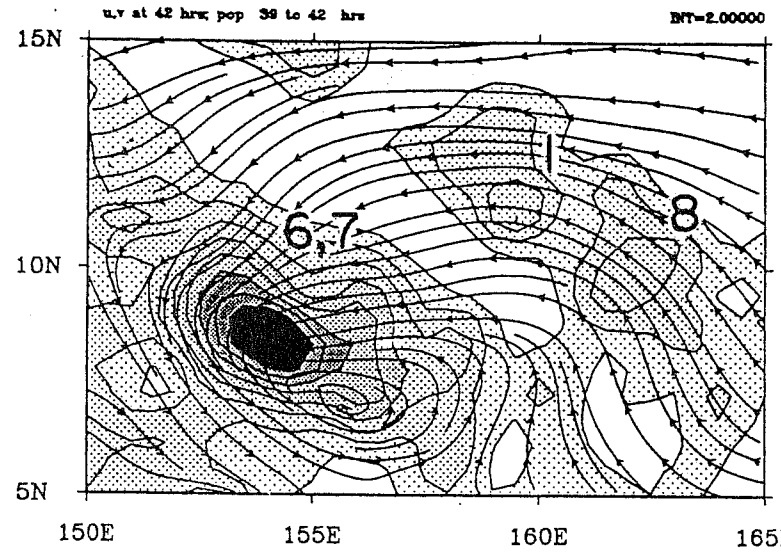

e

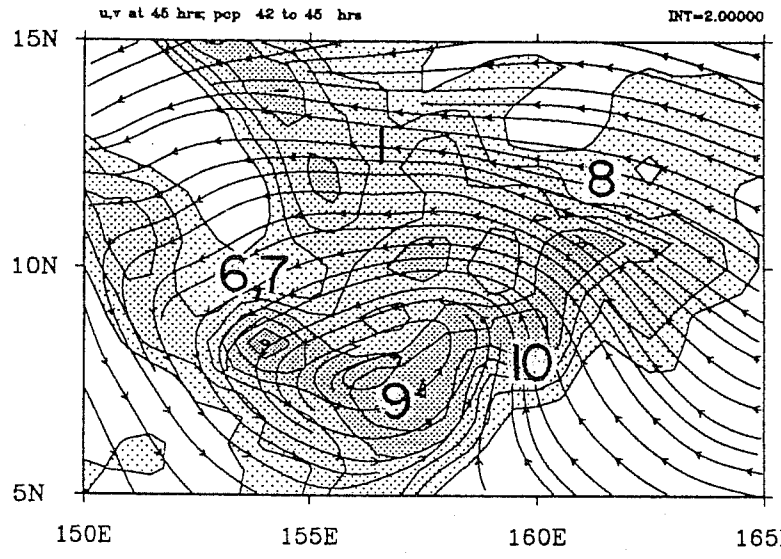

f

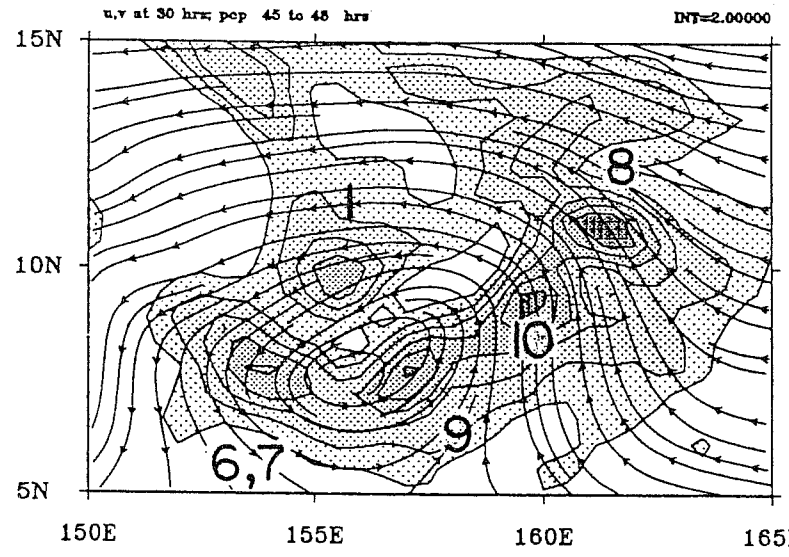

g

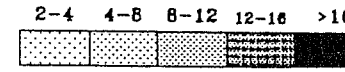

12 contd.

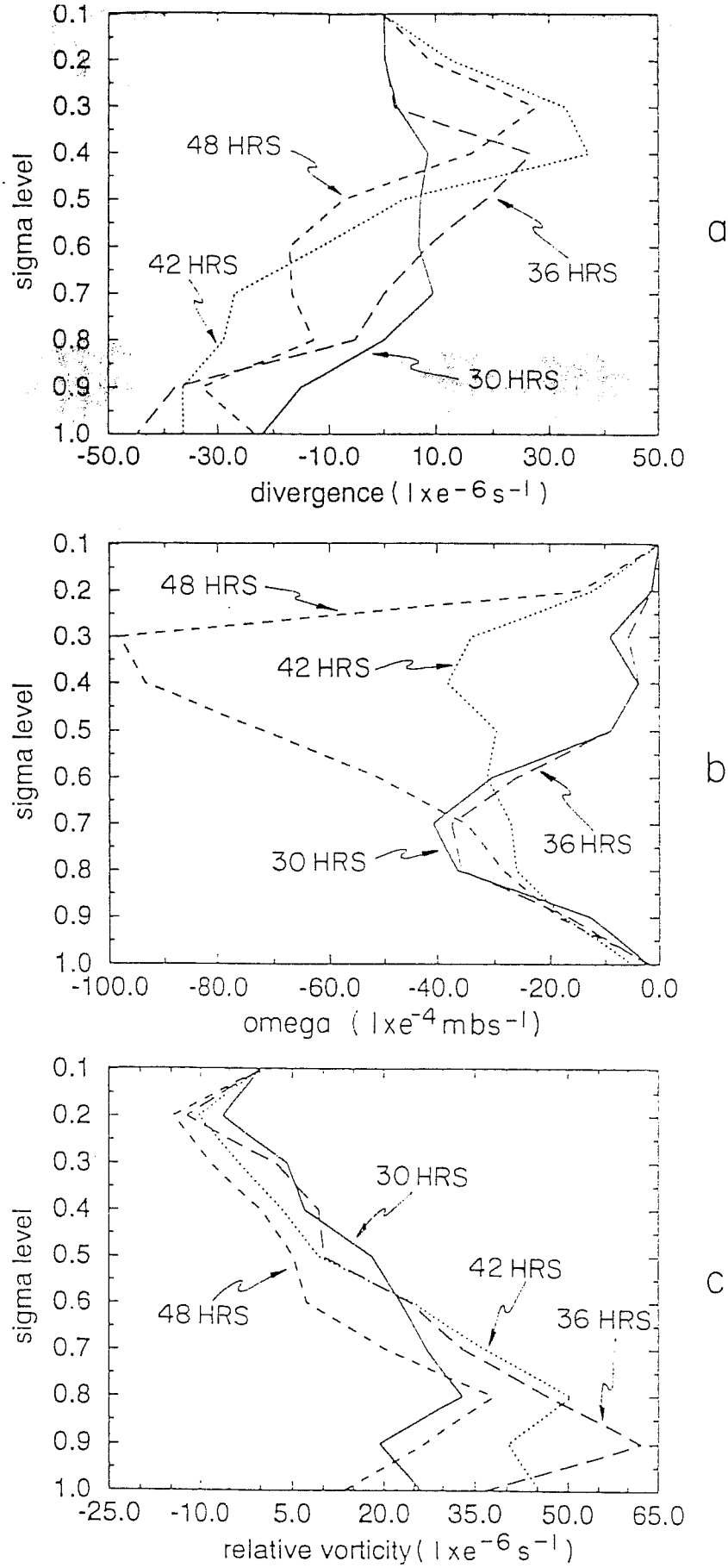

Fig (13) Time history following an individual meso-convective element between hours 30 and 48.

a) Vertical profile of divergence
b) Vertical profile of vertical velocity
c) Vertical profile of relative vorticity

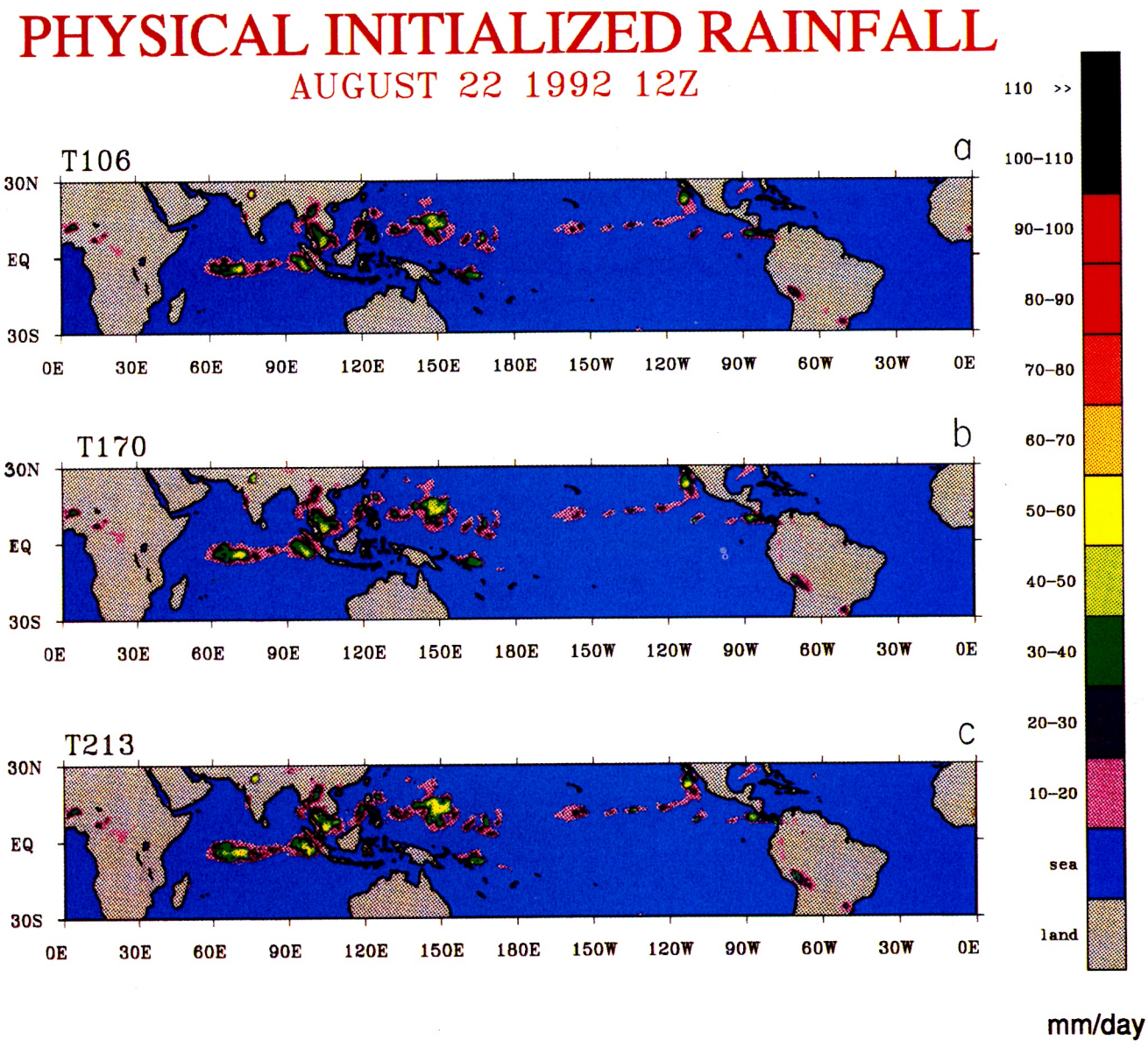

Fig (14) 24 hour physically initialised rainfall total (units mm/day) at different spectral resolutions a) T106, b) T170, c) T213.

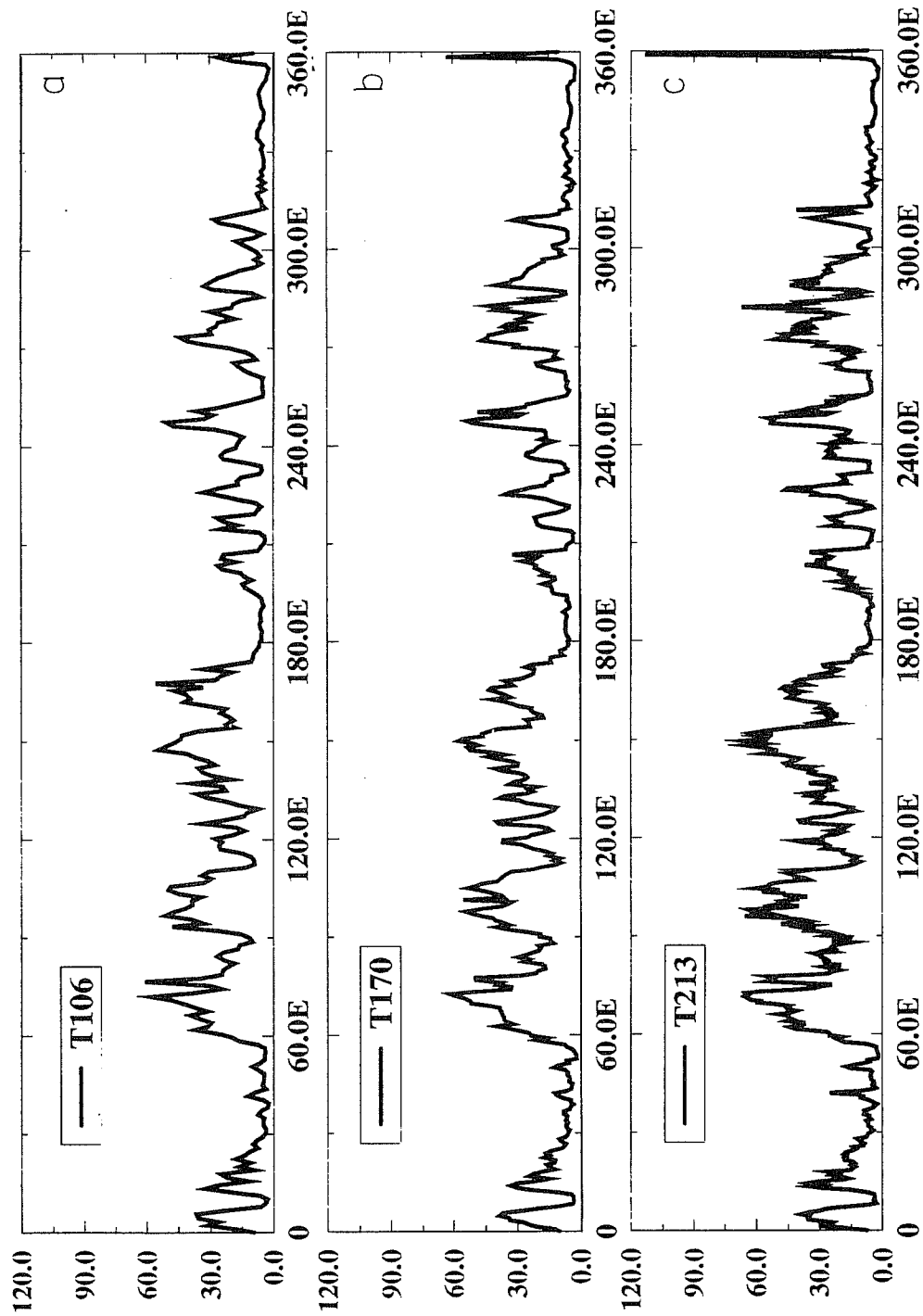

Fig (15) West east variation of physically initialized rainfall along a quasi-zonal line of maximum precipitation at different resolutions, (units mm/day). a) T106; b) T170; c) T213.

the match between the footprint of the SSM/ I data and the transform grid separation of the global model. As one follows the tropical axis of heaviest rainfall from west to east, the differences among the three different resolutions become more apparent. The graphs show large rainfall rates at the resolution T213 compared to the other resolutions. The spikes of larger rainfall at the resolution T213 denote the mesoscale systems (scales of the order of few hundred km) that can be followed in time within the high resolution model integrations.

The model at the high resolution exhibits the demise of the initial generation of meso-convective precipitating elements and the birth of a new generation of elements. The life span of these meso-convective elements is of the order of one day. The model's one day forecast skill (Figure 4) is quite high (correlation of 55% for the observed versus predicted rain) and demonstrates that meso-convective elements are in fact being advected reasonably in the high resolution global model. The high skill of the rainfall covers some 40 to 50 meso-convective precipitating clusters.

An important question is raised in reference to the future of modeling. There is a large thrust to expand the scope of nonhydrostatic very high resolution models including microphysical processes. To address meso-convective elements whose scales are of the order of few hundred kilometers, a non-hydrostatic model with explicit cloud physics, with a grid resolution of the order of a kilometer may be minimally necessary. Prediction of such elements would require the definition of the initial state at these resolutions. Lacking adequate 3-dimensional definition of the initial state, forecast error will no doubt be present. The question arises whether such models could have nowcasting and one day forecasting skill above these seen in Figure (4). To achieve such skills over the entire tropics the computing and initial data requirements would be exceptionally demanding for the non-hydrostatic models. That appears to be the future direction of mesoscale modeling. For the present the implicit methods for the handling of convective processes may be competitive with the explicit nonhydrostatic microphysical models for the handling the entire tropics.

6. THE IMPROVEMENTS OF HYDROLOGICAL BUDGETS:

The Bangladesh region encounters some of the most severe floods on an annual basis. Although floods are more common in the monsoon months, June through early September, flooding related to the passage of tropical depressions and tropical storms have been historically more catastrophic. Estimates of hydrological budgets during such episodes can be accomplished with an improved consistency among the estimates of moisture convergence, evaporation and the observed rain rates with the physical initialization. An example of an episodic nature of these flooding events will be illustrated. If a short duration event such as the passage of a tropical depression causes heavy flooding, then useful interpretation of the hydrological

budget can only be obtained by focusing on the duration of that event. Use of month long data sets can be somewhat misleading.

We carried out physical initialization for the entire month of October, 1991, during this month a post-monsoon season flooding event occurred which in fact lasted for roughly 4 days between October 11 to October 14. This was related to the passage of a monsoon depression that formed over the Bay of Bengal along the ITCZ at roughly 15N and moved northwards. Figure (16) shows the 850 mb circulation illustrating its northward passage. On the eastern flank of this storm the southerly flow brought in a large amount of moist air from the Bay of Bengal. The convergence of flux of this moist air, during this period, resulted in substantial rainfall and flooding.

The daily history of the evaporation, precipitation, rain rates and convergence of the flux of moisture for the Bangladesh region are shown in Figure (17). This includes the results for the entire month of October, 1991. Krishnamurti et al. (1994) examined this period in some detail and demonstrated that physical initialization with a high resolution global model provides a consistency among the elements of the hydrological budget. The estimates of evaporation presented are based on surface similarity theory which invokes stability dependent exchange coefficients. Also included is a low wind speed correction, based on Beljaarsand Miller (1990) for the exchange coefficients. This involves vertical eddy turbulent kinetic energy in its estimates of the exchange coefficients for wind speeds less than 5ms-1. The rain rate estimates come from the previously mentioned mixed algorithm (Gairola and Krishnamurti, 1992).

If one considers the hydrological budget for the entire month of October 1991, an entirely different perspective is obtained compared to what was found for the period of the flooding, October 11 through 14. October is usually a dry post-monsoon month over the Bangladesh region. The hydrological budget based on month long data for this region is shown in Figure (18a). A divergence of the flux of moisture is noted along with a decrease in the total precipitation (for the entire month of October). That picture does not convey the heavy flood which was a short duration episode. If one looks at the hydrological budget of the episode, averaged over the 4 days (October 11 through 14) we find a net convergence of flux of moisture, a moistening within the column enhancement of total precipitable water and precipitation exceeding the net evaporation, Figure (18b). This appears to reflect the flooding situation better than using the entire month of data. During this period flooding was experienced at x, y and z. The following tributaries of the Ganges, A, B and C exceeded above flood level waters.

7. ENSEMBLE FORECASTS OF TROPICAL CYCLONE TRACKS

The use of observed rain rates within physical initialization modifies the definition of divergence (the divergent wind), the vertical distribution of latent heating and moisture and the pressure tendency throughout the assimilation period. If several different analyses from diverse data assimilation groups were

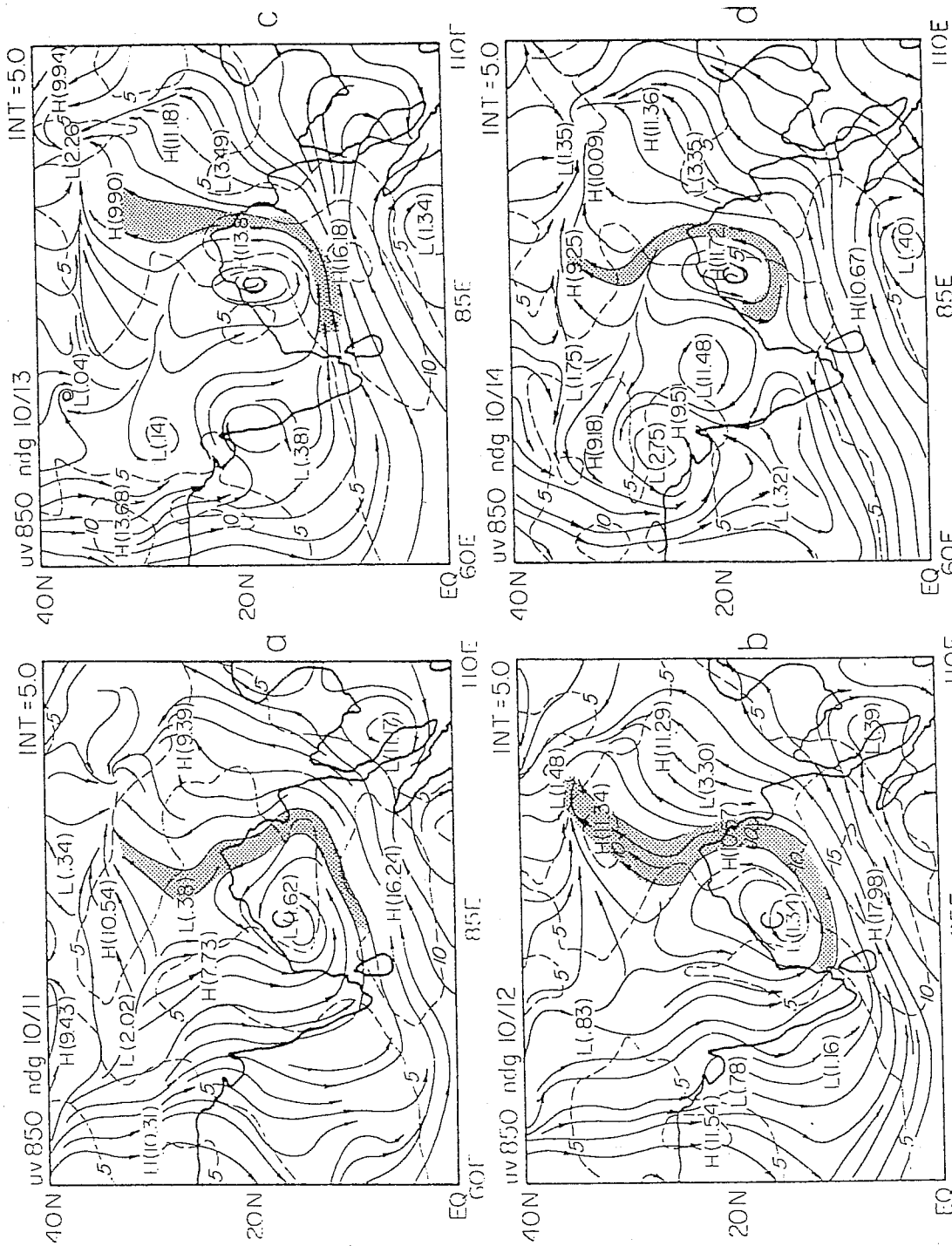

Fig (16) 850 mb circulations for October 11, 12, 13 and 14, 1991 at 12UTC streamlines: solid lines; isotachs: dashed lines (ms^{-1}).

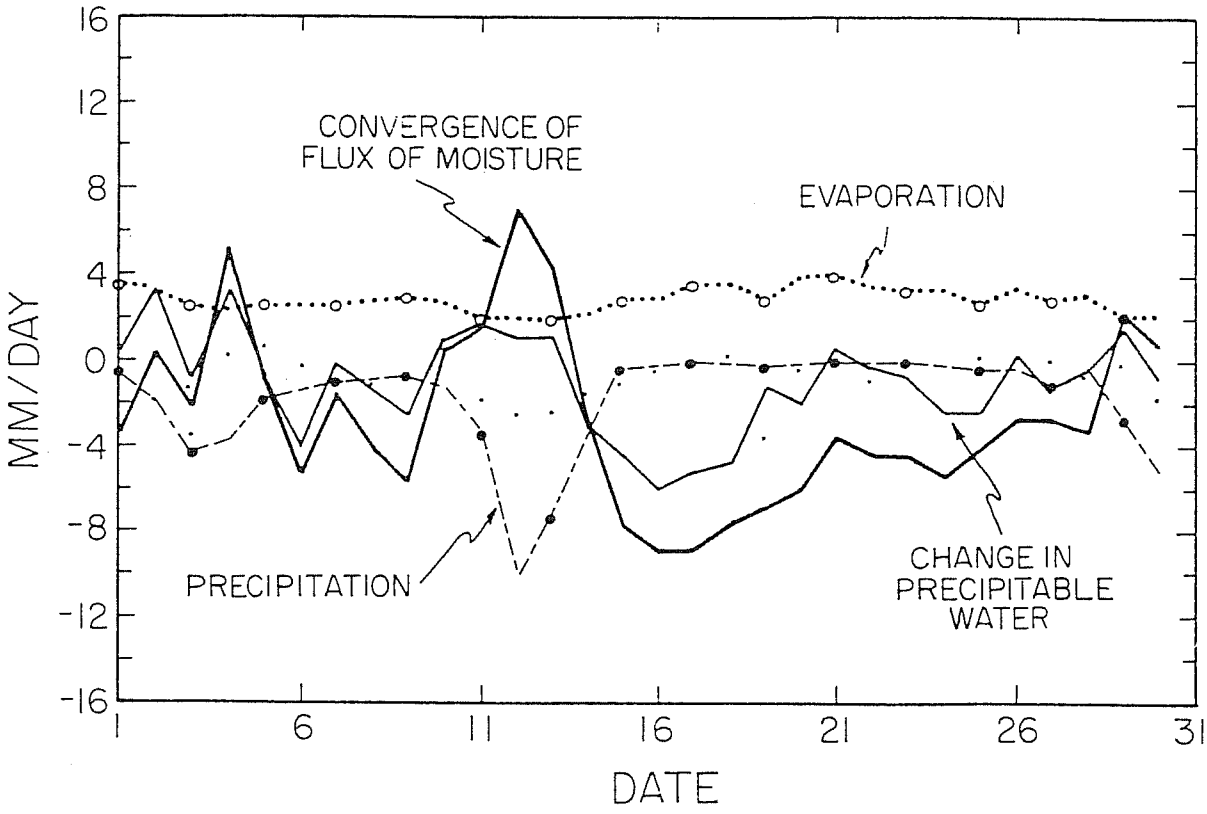

Fig (17) Daily time history of the hydrological budget components during October 1991 over Bangladesh. The different components are labeled in the diagram. The unconnected dots denote the diffusion terms.

WATER BUDGET OCTOBER 1991

BANGLADESH

$$\frac{\delta \bar{q}}{\delta t} = -\overline{\nabla \cdot \nabla q} + E - P + (Res.)$$

$-1.25 = -2.69 + 2.95 - 1.75 + (0.24)$ mm/day

$5.33 = -11.48 + 12.58 - 7.48 + (1.05) \times 10^8$ mton/day

a

MOISTURE CONVERGENCE BUDGET

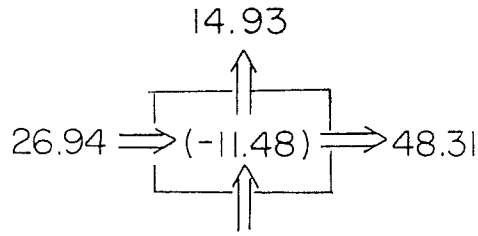

$\times 10^8$ mton/day

WATER BUDGET 11-14 OCTOBER 91

$$\frac{\delta \bar{q}}{\delta t} = \overline{-\nabla \nabla q} + E - P + (Res.)$$

$0.15 = -2.51 + 2.45 - 6.00 + (1.19)$ mm/day

$0.63 = 10.72 + 10.45 - 25.62 + (5.08) \times 10^8$ mton/day

b

MOISTURE CONVERGENCE BUDGET

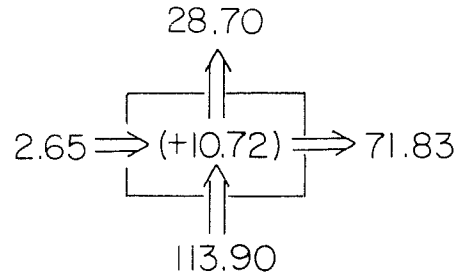

Fig (18) Hydrological budget over the Bangladesh region a) month long data sets, October 1991. b) For the period of heavy rains, October 11 to 14, 1991.

subjected to physical initialization, using the same observed rain rate, one might expect to see a reduction of the spread of ensemble forecasts especially for tropical storm tracks. To examine this hypothesis 16 medium-range forecast experiments were completed. These include 8 control experiments and 8 which include the physical initialization. Among these we have 4 analyses, from NASA-GODDARD, NMC, ECMWF and GFDL at 0000 UTC and 4 analysis from each of these same groups at 12 UTC. Rain rates were prepared from a mix of OLR and raingauge similar to Gairola and Krishnamurti (1992) for a 24 hour period preceding the start times of the respective forecasts.

Figures (19 a, b) illustrate the spread of predicted tracks for Hurricane Frederic of 1979 with and without physical initialization.

The left panels in these illustrations show the forecasts for the control experiments and the right panels show the results from forecasts that include physical initialization. It is clearly apparent from these forecasts that the ensemble spread for the medium range forecasts is considerably reduced by the inclusion of physical initialization. This improvement has come from the incorporation of similar initial information on divergence, convective heating, moisture and surface pressure tendency for the entire ensemble of 8 experiments.

The forecast skill of these experiments were evaluated. The position errors for the storms are calculated by averaging the forecast positions of the ensemble members and calculating the difference between ensemble-averaged positions (outlier forecast tracks were excluded in the averaging process) and the best track positions provided by the National Hurricane Center and Joint Typhoon Warning Center. We noted that the forecasts which included the physical initialization reduced the position errors when compared to the control forecasts.

8. CONCLUDING REMARKS

Physical initialization appears to be a powerful procedure for the nowcasting and short range forecasting of tropical precipitation. This procedure incorporates additional observations over the data sparse tropics. These data are the observed precipitation measurements obtained from surface raingauges and the satellite based indirect estimates of rain rates which come from OLR and the microwave radiometer. The physical initialization enhances the definition of meso scale divergence, vorticity, vertical motion, convective heating and the surface pressure tendencies.

Physical initialization can only be as good as the rain rates we provide to its reverse algorithms and to the formulations of physical parameterizations. In spite of that major limitation within a prescribed set of rainfall input and prescribed parameterizations of physical processes, the method appears to enhance the quality of tropical initialization and short range prediction markedly. Physical initialization appears to

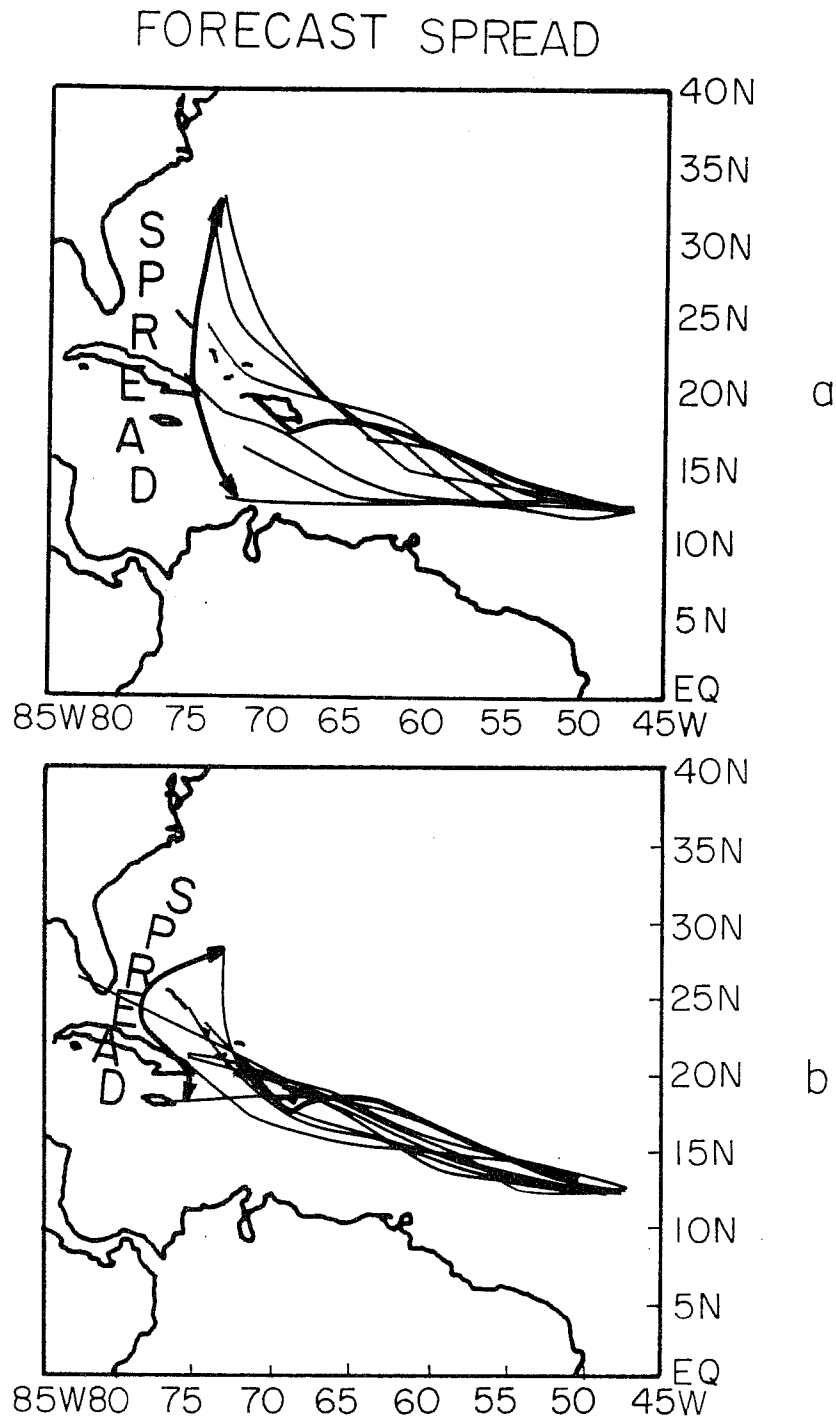

Fig (19) Ensemble forecasts for hurricane Frederic of 1979 over the Atlantic ocean. Start dates are September 1, 1979. Predicted trades are based on different initial analysis. The spread of forecasts on day 6 are highlighted.

provide skills above those of the operational centers for nowcasting and short-range prediction over the tropics.

We note also that for a high resolution global model, such as T213, the separation of the transform grid matches roughly the footprint of the SSM/I. Thus, the physical initialization appears to capture the initial and the subsequent motions of meso-convective precipitating elements quite well. Since most of the rainfall occurs from the passage of meso-convective elements, at this resolution we see a higher skill for the one day rainfall forecasts from the passage of these meso-convective elements. In this context, we illustrate the development of Typhoon Omar of 1992 which developed from a tropical depression. We show an interesting organization of convection into a near circular geometry. This contributed to the initial development of Typhoon Omar. It had been difficult to see such meso-scale contributions to storm developments from coarse resolution models.

Physical initialization appears to provide a consistency among the precipitation, evaporation, convergence of the flux of moisture and the local changes in the precipitable water. The improvements in the convergence of the flux of moisture arise from the improvements in the definition of the divergent component of the wind and the vertical variations of the humidity variable. As a consequence, it has been possible to improve the computations of hydrological budgets. This was illustrated for a short duration Bangladesh flood event. Such budgets executed from data sets that are not initialized for the observed rainrate fail to define the correct sign of the moisture convergence - largely due to data inadequacies.

We have seen a benefit of physical initialization for ensemble forecasts of hurricane tracks. The spread of an ensemble of track forecasts is reduced. That reduction is related to the fact that all members of the ensemble are subjected to the rainrate input in the physical initialization. That enrichment of the similar additional data (divergence, convective heating and moisture) for each member acts to limit the spread somewhat.

The future of physical initialization must lie in a proper implementation of this entire process within a four-dimensional variational assimilation where the adjoints for the precipitation processes need to be incorporated requiring that the reverse algorithms incorporate the observed rain rates.

9. ACKNOWLEDGMENTS

The work reported here was supported by the following grants: NSF ATM 9312537, ONR 00014-93-10243, NASA 37 WA 0361, NOAA NA 37WA0361. Computations reported here were carried out on the CRAY YMP's at NCAR and FSU.

10. REFERENCES

Beljaars, A., and M. Miller, 1990: A note concerning the evaporation from the tropical oceans: sensitivity of the ECMWF model to the transfer coefficient of moisture at low wind speed. ECMWF Research Department Technical Memo 170, ECMWF, Reading, 19 pp.

Goirala, R.K. and T.N. Krishnamurti, 1992: Rain rates based on SSM/I, OLR and raingauge data sets. J. Meteorol. Atmos. Phys., 50, 165-174.

Holland, G.J. and G.S. Dietachmayer, 1993: On the interaction of tropical-cyclone-scale vortices. III: Continuous barotropic vortices. Quart. J. Roy. Met. Soc., 119, 1381-1391.

Krishnamurti, T.N., S.K.R. Bhowmik, D. Oosterhof, G. Rohaly and N. Surgi, 1995: Meso-scale structure implied by physical initialization. (Submitted to Monthly Weather Review).

Krishnamurti, T.N., G. Rohaly and H.S. Bedi, 1994: On the improvement of precipitation forecast skill from physical initialization. Accepted for publication in Tellus.

Krishnamurti, T.N., H.S. Bedi and K. Ingles, 1993: Physical initialization using SSM/I rain rates. Tellus, 45A, 247-269.

Krishnamurti, T.N., J. Xue, H.S. Bedi, K. Ingles and D. Oosterhof, 1991: Physical initialization for numerical weather prediction over the tropics. Tellus, 43AB, 53-81.

Kummerow, C. and L. Giglio, 1994: A passive microwave technique for estimating rainfall and vertical structure information from space. Part 1: Algorithm description. J. Appl. Meteorology, 33, 3-18.

Lander, M. and G.J. Holland, 1993: On the interaction of tropical-cyclone-scale vortices. I: Observations. Quart. J. Roy. Met. Soc., 119, 1347-1361.

Lee, H.S. and T.N. Krishnamurti, 1994: Impact of Physical initialization on cloud forecasts. J. Meteor. Atomos. Physics. To be published.

Olson, W.S., F.S. Fontaine, W.L. Smith and R.H. Achtor, 1990: Recommended algorithms for the retrieval of rainfall rates in the tropics using SSM/I (DMSP-F8). Manuscript, University of Wisconsin, Madison, 10pp.

Parsons, D., Dabberdt, W., Cole, H., Hock, T., Marin, C., Barrett, A., Miller, E., Spowart, M., Howard, M., Ecklund, W., Carter, D., Gage, K., and Wilson, J., 1994: The Integrated Sounding System: Description and Preliminary Observations from TOGA COARE. Bull. of the Am. Met. Soc., 75, 553-568.

Ritchie, E.A. and G.J. Holland, 1993: On the interaction of tropical-cyclone-scale vortices. II: Discrete vortex. Quart. J. Roy. Met. Soc., 119, 1363-1379.

Spencer, R.W., 1993: Global oceanic precipitation from MSU during 1979-91 and comparison to other climatologies. Journ. of Climate, 6, 1301-1326.

Tiedke, M., 1984: The sensitivity of the time-mean large-scale flow to cumulus convection in the ECMWF model. Workshop on Convection in large-scale numerical models. ECMWF, 28 Nov. -1Dec. 1983, 297-316.

Yanai, M., Esbensen, S. and Chu, J.H., 1973: Determination of bulk properties of tropical cloud clusters from large-scale heat and moisture budgets. J. Atmos. Sci., 30, 611-627.

11. TABLE 1. LIST OF ACRONYMS AND SYMBOLS

TOGA-COARE	TOGA-Coupled Ocean Atmospheric Response Experiment
$\hat{Q}_1$	Vertically integrated apparent heat source
$\hat{Q}_2$	Vertically integrated apparent moisture sink
$\hat{Q}_R$	Radiative heat source
OLR	Outgoing Longwave Radiation
SSM/I	Special Sensor Microwave Instrument
FSU	Florida State University
IOP	Intensive Observation Period
ISS	Integrated Sounding System
$\hat{E}$	Evaporation
$\hat{p}$	Precipitation
SST	Sea Surface Temperature
T106, T170, T214	Triangular Truncation at wave number 106, 170, 213
UTC	Coordinated Universal Time
ITCZ	Intertropical Convergence Zone
NMC	National Meteorological Center
NASA-GODDARD	National Aeronautic Space Administration, Goddard
ECMWF	European Center for Medium Range Weather Forecasts
GFDL	Geophysical Fluid Dynamics Laboratory
TOGA	Tropical Ocean and Global Atmospheric Program
IFA	Intensive Flux Array
GDAS	Global Data Assimilation System